16 Electrical Methods

Measurements of electrical properties of materials are of interest for diffusion experiments in several areas of materials science. *Impedance spectroscopy* plays an important rôle for ion-conducting materials. With the availability of commercially made impedance bridges covering wide frequency ranges impedance studies became popular among electrochemists and materials scientists. For an introduction to the field of impedance spectroscopy the reader may consult the textbook of MACDONALD [1]. In semiconducting materials electrically active foreign atoms have a strong influence on the electrical conductivity. For diffusion studies in semiconductors electrical measurements are useful. In particular *spreading resistance profiling*, introduced by MAZUR AND DICKEY in the 1960s [2], has become a powerful tool for measuring spatial distributions of electrically active atoms in semiconductors.

Electrical resistivity measurements on metals have sometimes also been used to study diffusion. These studies utilise the resistivity change that occurs upon in- or out-diffusion of foreign elements. This method is fairly indirect and diffusion profiles cannot be obtained. Therfore, we refrain from discussing such experiments.

16.1 Impedance Spectroscopy

In ion-conducting materials with negligible electronic conduction such as ionic crystals, ion-conducting glasses, and oxides the conductivity results from the hopping motion of ions. For such materials the measurement of the electrical conductivity is an indispensable complement to that of tracer diffusion. As discussed in Chap. 11, the dc conductivity, σ_{dc}, is related to the *charge or diffusivity*, D_σ, via

$$D_\sigma = \frac{\sigma_{dc} k_\mathrm{B} T}{N_{ion} q^2} \,. \tag{16.1}$$

N_{ion} denotes the number density of mobile ions and q the electrical charge per ion.

Measurements of the ionic conductivity are carried out with an ac bridge to avoid polarisation effects at the electrodes. An experimental set-up is illustrated in Fig. 16.1. The measurements are usually made with cells which have

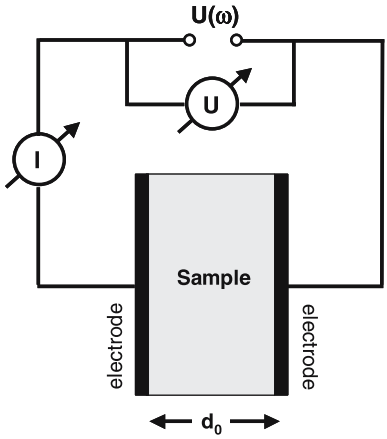

Fig. 16.1. Schematic illustration of an impedance bridge with sample and electrodes

two identical electrodes applied to the faces of a sample in the form of a circular cylinder or rectangular parallelepiped. The general approach is to apply an electrical ac stimulus of frequency ν (a known voltage or current) and to observe the resulting response (current or voltage). Usually, impedance spectroscopy can cover a frequency range from about 10^{-3} Hz to several MHz. The experimental set-up requires a variable frequency generator and a vector ammeter and volt-meter for current and voltage measurements including the phase-shift between current $\hat{I}(\nu)$ and voltage $\hat{V}(\nu)$. The complex impedance is defined as

$$\hat{Z}(\nu) \equiv \frac{\hat{V}(\nu)}{\hat{I}(\nu)} . \tag{16.2}$$

It is composed according to

$$\hat{Z}(\nu) = Z' - iZ'' \tag{16.3}$$

of real and imaginary parts, Z' and Z''. i denotes the imaginary unit. The complex conductivity

$$\hat{\sigma}(\nu) = \sigma'(\nu) + i\sigma''(\nu) \tag{16.4}$$

is also composed of a real part, σ', and an imaginary part, σ''. Conductivity and complex impedance are related via

$$\hat{\sigma}(\nu) = \frac{1}{\hat{Z}(\nu)} \frac{d_0}{A} , \tag{16.5}$$

where d_0 and A denote the thickness and the electrode area of the sample, respectively.

For a discussion of impedance measurements, it is convenient to recall that the complex impedance of a circuit formed by an ohmic resistance R and a capacitance C parallel to it is given by

$$\hat{Z} = \frac{R}{1 + i\omega CR}\,, \tag{16.6}$$

where $\omega = 2\pi\nu$ denotes the angular frequency. Then, the real and imaginary parts of the impedance can be written as

$$Z' = \frac{R}{1 + \omega^2 R^2 C^2} \quad \text{and} \quad Z'' = \frac{\omega C R^2}{1 + \omega^2 R^2 C^2}\,. \tag{16.7}$$

The representation of the impedance in the complex $Z' - Z''$ plane is denoted as the *Cole diagram*. For a RC-circuit the values of $\hat{Z}(\omega)$ plotted in the Z' versus $-Z''$ plane fall on a semicircle of diameter R, passing through the origin for $\omega \to \infty$, through $(R, 0)$ for $\omega = 0$, and through $(R/2, R/2)$ for $\omega = (RC)^{-1}$.

When several circuits of this type are connected in series, the graphic representation is a series of semicircles as illustrated in Fig. 16.2. An ensemble of three RC circuits in series can represent a measurement cell. The cell may consist of a polycrstalline sample plus electrodes. Each circuit represents a conductivity process: R_V and C_V volume conduction, R_b and C_b boundary conduction, and R_e and C_e the electrode process. One should, however, keep in mind that the representation of the total impedance of an experimental set-up by RC-circuits can be oversimplified. Sometimes other equivalent circuits may better represent the actual processes. Furthermore, sometimes the centers of the arcs are below the Z'-axis.

As a simple experimental example, Fig. 16.3 shows the Cole diagram for an ion-conducting alkali-borate glass according to Imre et al. [3]. The semicircles represent the volume conduction process at various temperatures. Grain boundaries are absent in a glass and the electrode process is located at lower frequencies not displayed in the figure. The dc resistance of the sample is given by the intercept of the arcs with the Z'-axis. It decreases with increasing temperature. The dc conductivity can be deduced from the ohmic resistance observed at the intersection of the 'semicircle' with the Z'-axis of Fig. 16.3. The real part of the conductivity times temperature ($\sigma' \times T$) of the same material is shown in Fig. 16.4 as a function of the frequency ν for various temperatures. The low frequency plateau in Fig. 16.4 corresponds to the dc conductivity. This plateau reflects the long-range transport of ions. The dc-conductivity increases with temperature Arrhenius activated.

Using relation Eq. (16.1), the *charge diffusivity*, D_σ, can be deduced (see Chap. 11). This quantity is displayed in the Arrhenius diagram of Fig 16.5 together with the tracer diffusivity of ^{22}Na measured on the same material according to [4]. As discussed in Chap. 11 the ratio between tracer diffusivity D^* and the conductivity diffusivity is denoted as the *Haven ratio*, $H_R \equiv$

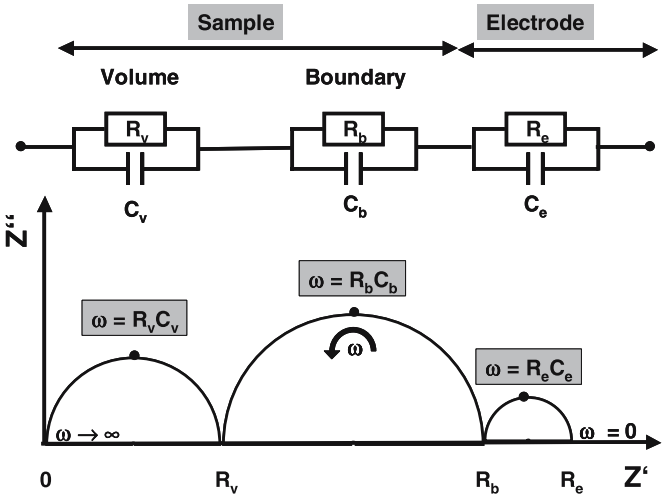

Fig. 16.2. Circuits for the complex impedance and Cole diagram

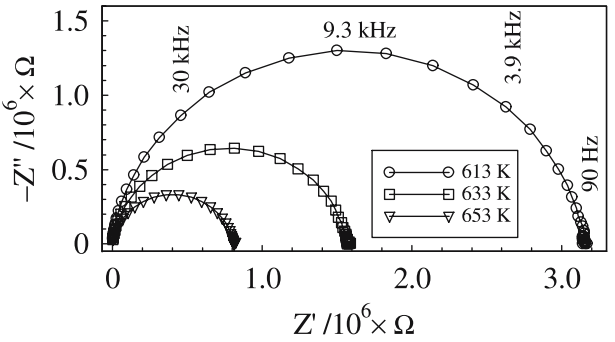

Fig. 16.3. Complex impedance (Cole diagram) for three temperatures representing volume conduction of a sodium-borate glass [3]

D^*/D_σ, which is usually less than unity. A measurement of the Haven ratio can provide useful information about the atomic mechanism of diffusion and the correlation effects involved. In the illustrated case, the Haven ratio is temperature-independent indicating that the mechanism of ionic motion does not change with temperature.

The increase of the conductivity at higher frequencies is called dispersion. The conductivity dispersion reflects the fact that ionic jumps are correlated (see, e.g., [5]). An onset frequency of dispersion, ν_{onset}, may be defined by the condition $\sigma'(\nu) = 2\sigma_{dc}$. The fact that the onset frequencies in Fig. 16.4 lie on a straight line with a slope of unity shows that $\sigma_{dc} \times T$ and ν_{onset} are thermally activated with the same activation enthalpy. This behaviour is sometimes denoted as Summerfield scaling [6]. Microscopically, it implies

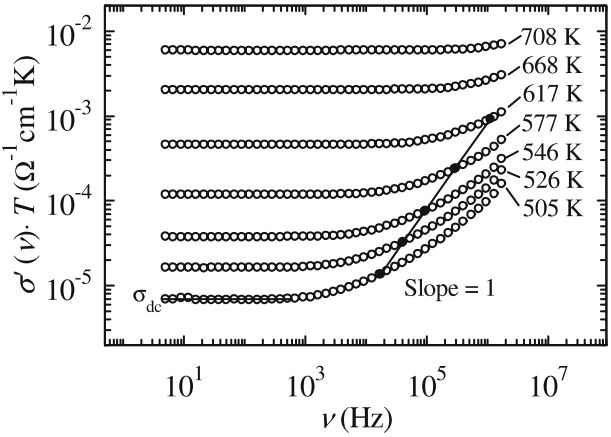

Fig. 16.4. Conductivity spectra of a sodium borate glass in a diagram of logarithm $\sigma' \times T$ *versus* logarithm of the frequency ν. The onset frequencies of dispersion for various temperatures are connected by a *straight line*

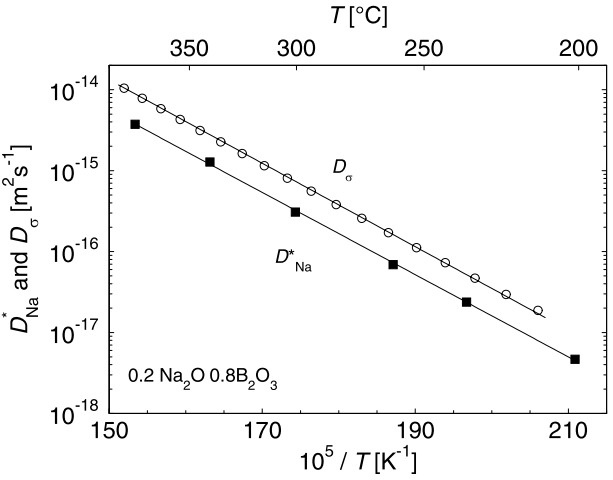

Fig. 16.5. Arrhenius diagram of the charge diffusivity D_σ and the tracer diffusivity D^* of ^{22}Na for a sodium borate glass

that the same jump processes occur at different temperatures. Of course, their jump rate is higher at higher temperatures. Summerfield scaling is observed for several materials but by no means in all ion conducting materials. For more information about conduction in disordered ionic materials the reader may consult Chap. 30 and reviews, e.g., by Ingram [7], Dieterich and Maas [8], Funke and coworkers [9], and by Bunde et al. [10].

16.2 Spreading Resistance Profiling

In semiconductors, the resistivity in the extrinsic domain is related to the concentration of electrically active foreign atoms. The concentration distribution of such atoms can be deduced by measuring the spreading resistance R_s (see below). Spreading resistance profiling (SRP) [2] has become a useful tool for measuring spatial distributions of electrically active atoms in semiconducting samples. SRP is widely used in silicon technology to monitor depth profiles of dopants after processing steps and to check the lateral uniformity in the resistivity of virgin Si wafers. In addition, SRP has been successfully applied in basic studies of diffusion processes in Si (see, e.g., [11, 12]), in Ge [13] and to a lesser extent in GaAs [14].

SRP is a two-point-probe technique, which measures the electrical resistance on semiconductor surfaces with a much higher spatial resolution than the traditional four-point-probe technique. The concentration-depth profile for foreign atoms can be established by measuring the resistance of the sample between two 'points' as indicated in Fig. 16.6. The probe tips, usually made of a tungsten-osmium alloy, are separated by a distance of typically 100 µm or less. The current between the probes spreads over a small space region near the semiconductor surface, which explains the notion 'spreading resistance'. A SRP device is commonly operated in an automatic-stepping mode with probe-tip steps varying from 5 to 25 µm. The measurements can be either performed on a cross section of the sample or for shallow profiles on a bevelled section as indicated in Fig. 16.6. An example for an experimental spreading resistance profile is displayed in the left part of Fig. 16.7. The right part shows the concentration-depth profile deduced from the spreading resistance profile. The employed procedure is described below.

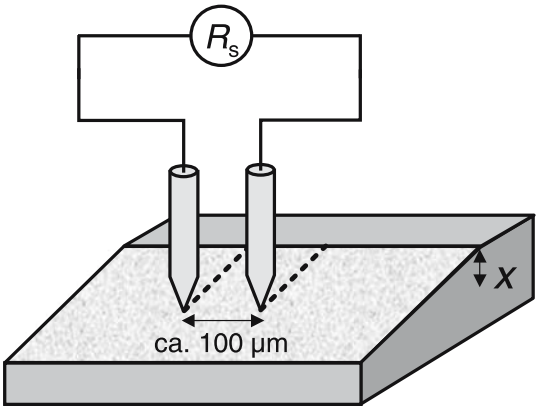

Fig. 16.6. Spreading resistance profiling (schematic)

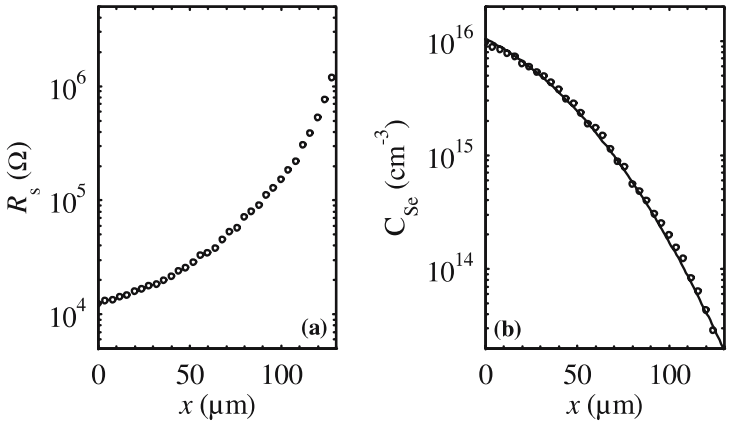

Fig. 16.7. Spreading resistance profile of Se in Si (*left*) and concentration depth profile of Se deduced therefrom (*right*)

The SRP technique relies on the fact that the ideal resistance of a small-diameter metal probe in perfect contact with the plane surface of a semi-infinite semiconductor is given by

$$R_s = \frac{\rho}{4a}\,, \tag{16.8}$$

where ρ denotes the resistivity of the semiconductor and a the radius of the contact area. The spreading resistance, R_s, originates from the radial flow of the current from the probe tip into the semiconductor. Due to the special configuration, about 80 % of the potential drop occurs within a distance of $5a$. In practice, the SRP contact radius can be made as small as a few μm, which leads to a corresponding small sampling volume. Theoretically, the two-probe arrangement doubles R_s with regard to Eq. (16.8), provided that the probe-tip separation is much larger than the contact radius. In reality, the contacts are not planar circles but irregularly shaped microcontacts. This gives rise to substantial contact resistance, which cannot be derived with sufficient accuracy from theory. Therefore, in SRP analysis the relationship between ρ and R_s is established by calibration using homogeneously doped samples of the same material, conductivity type, and surface orientation as the test sample under consideration.

Standard semiconductor theory is used to establish the relation between the resistivity and the concentration of the electrically active foreign atoms. We illustrate this procedure for a singly ionizable donor atom X in an otherwise undoped semiconductor. For a given Fermi energy E_F, the electron concentration n is obtained as

$$n = N_C \exp\left(\frac{E_F - E_C}{k_\mathrm{B}T}\right)\,, \tag{16.9}$$

where E_C denotes the energy of the conduction band edge and N_C the effective density of states in the conduction band. The latter quantity is closely related to the effective electron mass m_n according to

$$N_C = 2\left(\frac{2\pi m_n k_\mathrm{B} T}{h^2}\right)^{3/2}, \tag{16.10}$$

where h is the Planck constant. The hole concentration p follows from

$$np = n_i^2 = N_C N_V \exp\left[-\frac{E_G(T)}{k_\mathrm{B} T}\right] \tag{16.11}$$

with the intrinsic carrier density n_i, the temperature-dependent band gap energy, $E_G(T)$, and the effective density of states, N_V, in the valence band. Having obtained electron and hole concentrations, the charge neutrality condition

$$n = C_X^{ion} + p \tag{16.12}$$

yields the concentration C_X^{ion} of ionized foreign atoms. Values of C_X^{ion} distinctly above $10^{-16}\mathrm{cm}^{-3}$ lead to enhanced scattering of charge carriers, which may be taken into account by expressions for the carrier mobilities of electrons $\mu_n = \mu_n(C_X^{ion}, T)$ and holes $\mu_n = \mu_n(C_X^{ion}, T)$. Empirical expressions of this kind can be found in the literature [15]. In a subsequent step the resistivity is obtained from

$$\frac{1}{\rho} = q\mu_n n + q\mu_p p\,, \tag{16.13}$$

where q denote the charge per carrier. For singly ionizable donor atoms the second term on the right hand side of Eq. (16.13) can be neglected for $C_X^{ion} \gg n_i$. Once the calculated resistivity $\rho(E_F, T)$ value has converged to the experimental one, E_F and $C_X^{ion}(E_F, T)$ are known. Then, the electrically neutral foreign atom concentration, C_X^0, results from

$$\frac{C_X^{ion}}{C_X^0} = g_X \exp\left(\frac{E_X - E_F}{k_\mathrm{B} T}\right). \tag{16.14}$$

This equation accounts for the electron occupation probability of a foreign atom with a donor level, E_X, and a degeneration factor, g_X. The latter equals 2 for common group-V dopants such as P in silicon. Finally, the total foreign atom concentration follows from

$$C_X = C_X^{ion} + C_X^0\,. \tag{16.15}$$

Background doping can be taken into account by including additional terms in the charge neutrality Eq. (16.12). The alternative case in which the foreign atom X has acceptor character can be treated in a similar set of equations reflecting the reversed rôle of holes and electrons as majority and minority charge carriers. For further details about SRP the reader may consult a paper by Voss et al. [16].

References

1. J.R. Macdonald (Ed.), *Impedance Spectroscopy – Emphasizing Solid Materials and Systems*, John Wiley and Sons, 1987
2. R.G. Mazur, D.H. Dickey, J. Electrochem. Soc. **113**, 255 (1966)
3. A.W. Imre, S. Voss, H. Mehrer, Phys. Chem. Chem. Phys. **4**, 3219 (2002)
4. H. Mehrer, A.W. Imre, S. Voss, in: *Mass and Charge Transport in Inorganic Materials II*, Proc. of CIMTEC 2002–10th Int. Ceramics Congress and 3^{rd} Forum on New Materials, Florence, Italy, 2002;, P. Vincenzini, V. Buscaglia (Eds.), Techna, Faenza, 2003, p.127
5. K. Funke, R.D. Banhatti, S. Brückner, C. Cramer, C. Krieger, A. Mandanici, C. Martiny, I. Ross, Phys. Chem. Chem. Phys. **4**, 3155 (2002)
6. S. Summerfield, Philos. Mag. B **52**, 9 (1985)
7. M.D. Ingram, Phys. Chem of Glasses **28**, 215 (1987)
8. W. Dieterich, P. Maass, Chem. Physics **284** 439 (2002)
9. K. Funke, C. Cramer, D. Wilmer, *Concept of Mismatch and Relaxation for Self-Diffusion and Conduction in Ionic Materials with Disordered Structures*, in: *Diffusion in Condensed Matter – Methods, Materials, Models*, P. Heitjans, J. Kärger (Eds.), Springer-Verlag, 2005
10. A. Bunde, W. Dieterich, Ph. Maass, M. Mayer, *Ionic Transport in Disordered Materials*, in: *Diffusion in Condensed Matter – Methods, Materials, Models*, P. Heitjans, J. Kärger (Eds.), Springer-Verlag, 2005
11. D.A. Antoniadis, A.G. Gonzales, R.W. Dutton, J. Electrochem. Soc. **125**, 813 (1978)
12. N.A. Stolwijk, J. Hölzl, W. Frank, Appl. Phys. A: Solid surf. **39**, 37 (1966)
13. H. Bracht, N.A. Stolwijk, H. Mehrer, Phys. Rev. B **43**, 14465 (1991)
14. G. Bösker, N.A. Stolwijk, U. Södervall, W. Jäger, H. Mehrer, J. Appl. Phys. **86**, 791 (1999)
15. C. Jacobini, C. Canali, G. Ottaviani, A. Alberigi Quaranta, Solid State Electron. **20**, 77 (1977)
16. S. Voss, N.A. Stolwijk, H. Bracht, J. Applied Physics **92**, 4809 (2002)